



Curcumin Loaded onto Magnetic Mesoporous Material MCM-41 for Controlled and Released in Drug Delivery System

Nidhal A. Atiyah^{a*}, Mohammed A. Atiya^b, Talib M. Albayati^b

^{a,c} Chemical Engineering Dept, University of Technology-Iraq, Alsina'a street, 10066 Baghdad, Iraq.

^b, Chemical Engineering, Al-Khwarizmi College of Engineering, University of Baghdad.

*Corresponding author Email: che.19.21@grad.uotechnology.edu.iq

HIGHLIGHTS

- Functionalization of MCM-41 using Fe₃O₄.
- Encapsulation of curcumin onto MCM-41, Fe₃O₄/MCM-41 and their characterization before and after modified and loaded with curcumin.
- Comparison of release profile of curcumin loaded onto MCM-41 and Fe₃O₄/MCM-41.
- Investigation of the release mechanism and release kinetics.

ARTICLE INFO

Handling editor: Qusay F. Alsahy

Keywords:

Curcumin
Drug Delivery System
Fe₃O₄/MCM-41
Kinetic adsorption
Loading and release
Magnetic

ABSTRACT

In this work, the mesoporous silica nanoparticles (MSNs) of type MCM-41 were manufactured and modified with Fe₃O₄ to load curcumin (CUR) CUR@Fe₃O₄/MCM-41 as an efficient carrier in drug delivery systems. X-ray diffraction (XRD), Scanning Electron Microscopy (SEM), Fourier Transform Infrared (FT-IR), and nitrogen adsorption-desorption isotherms were used to characterize the three samples: pure MCM-41, Fe₃O₄/MCM-41, & CUR@Fe₃O₄/MCM-41. Adsorption processes tests were carried out to determine the impact of various variables on the CUR load efficiency. These variables were the carrier dosage, pH, contact time, and initial CUR concentration. The maximal drug loading efficiencies (DL %) were 15.78 % and 22.98 %, respectively. According to the data, The Freundlich isotherm had a stronger correlation coefficient R²= 0.999 for MCM-41, while the Langmuir isotherm had a greater R² of 0.9666 for Fe₃O₄/MCM-41. A pseudo-second-order kinetic model fits well with R²=0.9827 for MCM-41 and 0.9994 for Fe₃O₄/MCM-41. Phosphate Buffer Solution (PBS) with a pH of 7.4 was utilized to study CUR release behavior. According to the research, the maximum release for MCM-41 and Fe₃O₄/MCM-41 might be 74.1 % and 25.19 % after 72 h, respectively. Various kinetic release models were used, including First-order, Korsmeyer-Peppas, Hixson and Crowell, Higuchi, and Weibull. After 72h, the drug release data were fit using a Weibull kinetic model with an R² of 0.944 and 0.764 for MCM-41 and Fe₃O₄/MCM-41, respectively.

1. Introduction

The most prevalent and widely acknowledged way of drug delivery is oral administration. Particles of mesoporous silica (MSPs) are gaining popularity as drug delivery carriers as they're convenient. As well as favored by patients [1-2]. Curcumin (CUR) is a polyphenol found in the rhizomes of a Curcuma longa plant and contains a wide range of pharmacological effects, including anti-carcinogenic properties against various cancers. Consequently, due to its low water solubility & bioavailability, this new compound's medicinal actions are limited [3]. Figure 1 shows the 2D structure of CUR, which was extracted from turmeric rhizomes (Curcuma longa) [4].

CUR was developed using nanotechnological techniques to improve its solubility & consequent bioavailability. Porous silica was already widely employed for biomedical applications & drug delivery scaling material for effective oral delivery of poorly water-soluble medicines for decades because of its numerous appealing features. The MCM- 41 is one of the mesoporous materials that have piqued the interest of many scientists as a potential drug delivery because of their huge pore volume, large specific surface area, highly ordered structure, tunable nanometer pores, and non-cytotoxic products [5-10].

Furthermore, there are silanol groups on the internal and external surfaces, making it easy to modify and more contact between the carrier & drug molecule, resulting in high drug loading [11]. A type of pharmaceutical, particle size, the releasing media, structure, and surface modification of a carrier surface are all factors that can influence drug loading ability and kinetics

of drug release [12]. The modified focuses on nanoparticles made of iron oxide; they are the most well-known nanoparticles in biomedical fields, with favorable bioactivity, manageable scale, a high level of durability, and potential uses. Magnetization has been a characteristic of nanoparticles. It can be used in various medical processes and isn't found in any other materials. Magnetic molecules improve immunoassay, isolation, Hyperthermia, drug administration, and Magnetic resonance imaging (MRI) [13]. Magnetic nanoparticle surface (MNPS) qualities allow control with an externally applied magnetic field to reach the desired tissues inside the human body and achieve the desired result [14].

Many researchers study CUR loading and release in a drug delivery system. For example, Harini et al. studied the CUR loaded and released on silica nanoparticles with Polyethylenimine functionalization. They found that CUR has a maximum loading efficiency of 80-90%. At the same time, the release of CUR in vitro was efficient at an acidic pH [15]. Taebnia et al. Investigated the CUR loaded and released on silica nanoparticles with amine functionalization. They found that CUR has a maximum efficiency of loading and ability (33.5 % in additional 0.45 mg drug/mg silica nanoparticles, correspondingly. CUR type AAS -MSNPs released 75.1 % of drug-loaded CUR type AAS -MSNPs in vitro after 48 hours at 37°C. [16]. No papers use functionalized MCM-41 with Fe₃O₄ for CUR drug loading by adsorption and release published.

This study aims to synthesize and characterize mesoporous materials MCM-41 then modify it with Fe₃O₄ according to the incipient wetness impregnation (IWI) process to improve the solubility of curcumin. The outcomes of different operational conditions were studied, including carrier doses, CUR concentrations, and contact times. It was also studied adsorption isotherms, kinetic adsorption, and kinetic release. In addition, CUR release activity is being investigated in Phosphate Buffer Solution (PBS) media at a pH of 7.4 and 37°C.

2. Materials and Procedures

2.1 Materials

Cetyl trimethylammonium bromide (CTAB) C₁₉H₄₂BrN, (Mw=364.45 g/mol), and Tetraethyl Orthosilicate (TEOS) (C₂H₅)₄SiO₄ with (Mw=208.3 g/mol) was provided from Sigma Aldrich in German. Curcumin has a molecular weight of 368.37 g/mol, and a molecular formula of C₂₁H₂₀O₆ was purchased from AVONCHEM Company for Pharmaceutical Industries in the UK. CDH India supplied potassium dihydrogen phosphate (KH₂PO₄) with 99.5 %, 136.2 Mwt. & dibasic potassium phosphate (K₂HPO₄), 98 %, 178.3 Mwt. Sasna Netherlands provided absolute ethanol (C₂H₅OH, 99 %, 46.07 Mwt.), hydrochloric acid (HCL) in 35–38 %, 36.46 Mwt. and sodium hydroxide (NaOH) with 95 %, 39.99 Mwt. No further purification of all chemical reagents that were used.

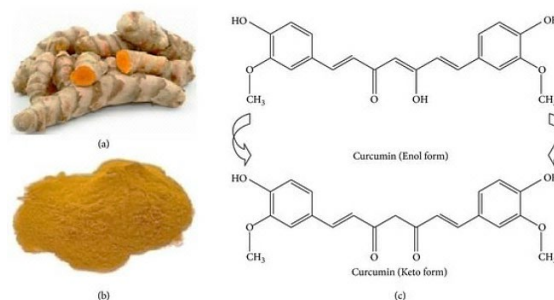


Figure 1: The 2D structure of CUR, which was extracted from turmeric rhizomes (*Curcuma longa*) [4]

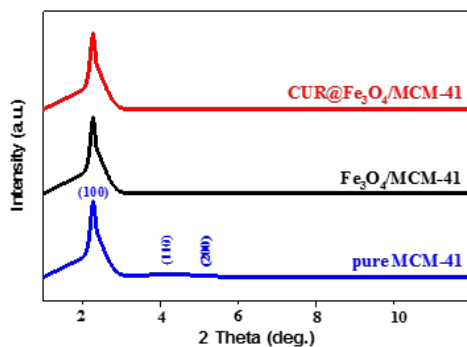


Figure 2: X-ray diffraction patterns for pure silica MCM-41, Fe₃O₄/MCM-41, & CUR@Fe₃O₄/MCM-41

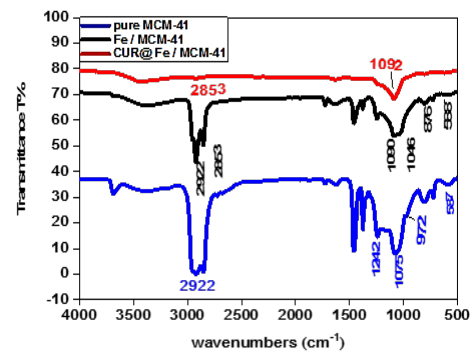


Figure 3: FTIR for pure MCM-41, Fe₃O₄/MCM-41 & CUR@Fe₃O₄/MCM-41

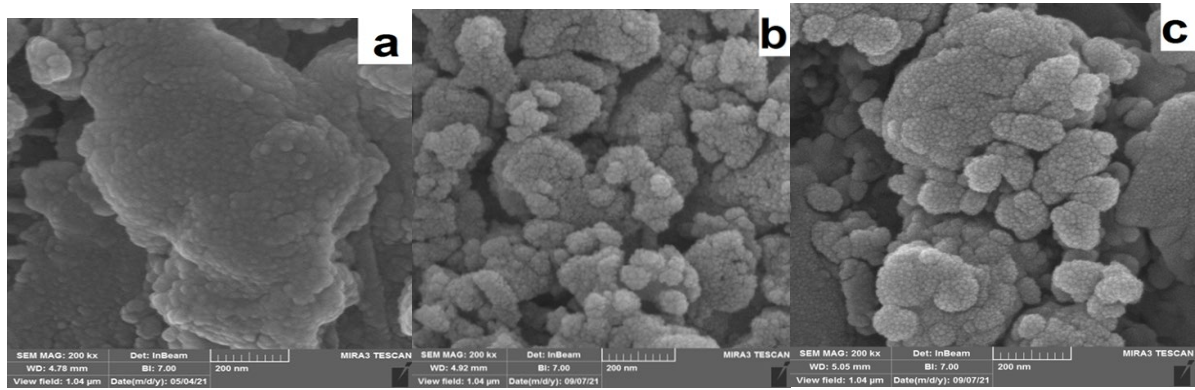


Figure 4: SEM image for (a) pure MCM-41(b) Fe₃O₄/MCM-41 and (c) CUR@Fe₃O₄/MCM-41

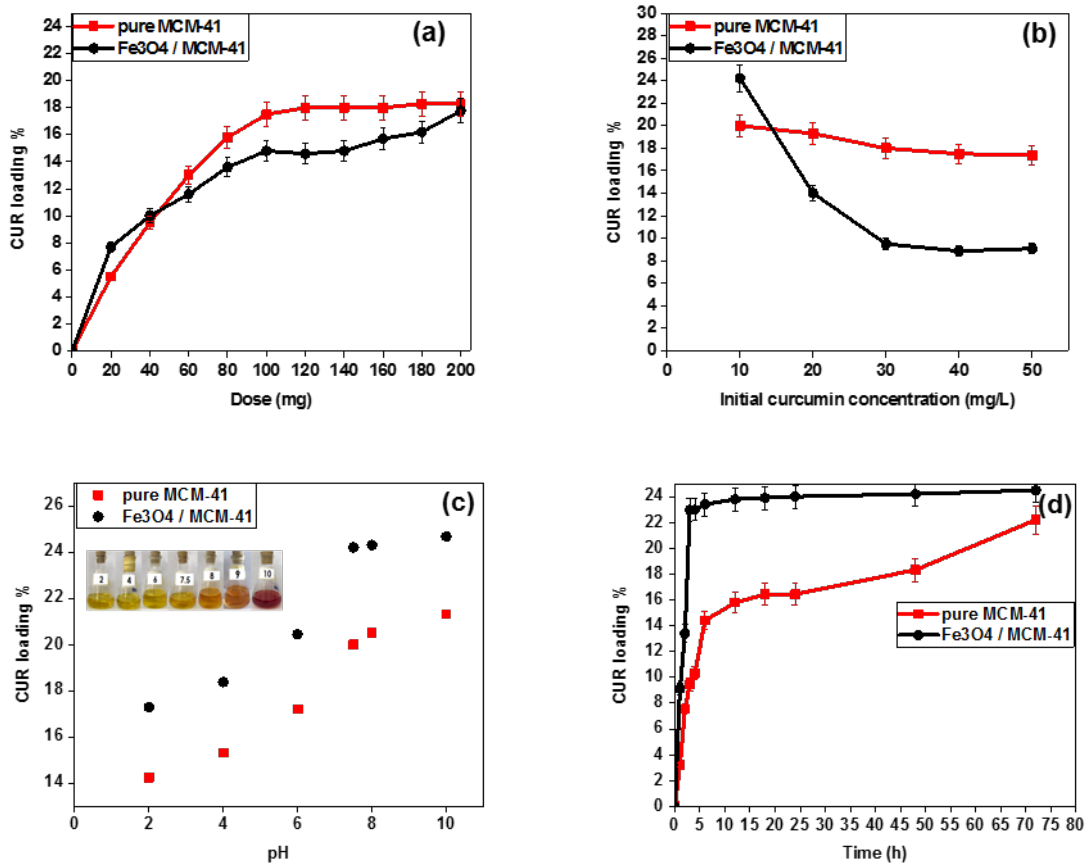


Figure 5: Effect of (a) dose (b) initial concentration (c) pH (d) contact time, on DL % for MCM-41 and Fe₃O₄/MCM-41, respectively

2.2 Synthesis of MCM-41 Mesoporous

The sol-gel method was used to produce MCM-41. The silica precursor was TEOS, and the structure-directing agent was CTAB. First, 1.01 g of CTAB was dissolved in a solution containing 0.34 g of NaOH and 30 ml of deionized water. Then, drop by drop, apply the added TEOS to the mixture with a weight of around 5.78 g when stirring at ambient temperature for one h. The homogeneous mixture output was crystallized in an autoclave for 96 h in constant hydrothermal conditions (110° C). Next, the solid product obtained via the filtration process was washed with deionized water to extract the partial surfactant. The obtained solid was then dried overnight at 40° C. Finally, the prototype was calcined at 550° C for six h to remove the surfactant. As a result of this process, a white powder MCM-41 was formed [17].

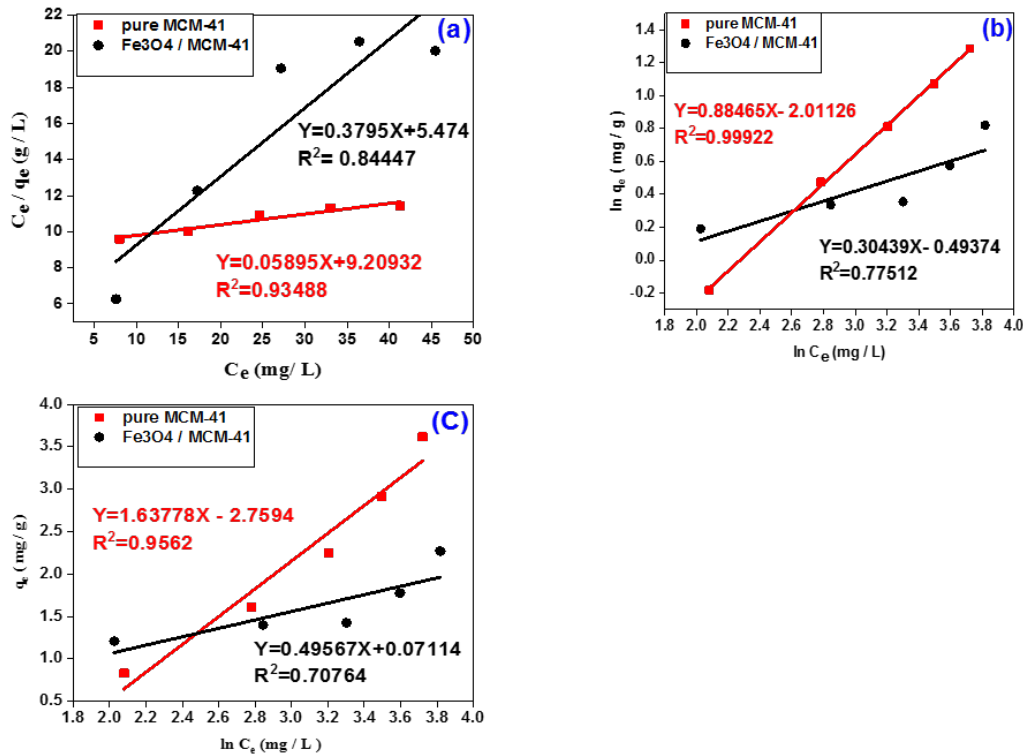


Figure 6: (a) Langmuir (b) Freundlich and (c) Temkin isotherm

2.3 Modification of the magnetic MCM-41

Magnetic mesoporous silica Fe₃O₄/MCM-41 was synthesized by adding Fe₃O₄ into MCM-41 using the Incipient Wetness Impregnation (IWI) process. For loading 1% of Fe₃O₄/MCM-41, 0.1960 g of Fe₃O₄ was added to 5 cm³ of HCL with a 35-38% concentration to make the impregnated solution. Then, 1.054 cm³ of the impregnated solution to 1gm MCM-41 was incorporated. The amount of Fe loaded accounted for 1% of the carrier's pore capacity. Then the magnetically mesoporous was impregnated and air-dried at room temp, after which it was then calcined in a furnace over four h at 300° C at a rate of 5°C/min [18][25].

2.4 Characterization

The X-ray diffraction (XRD-6000 Shimadzu) pattern was used to discover a crystal structure and calculate characteristics with 2θ in the range 0° – 10° with only a scan rate of 2 (deg/min) for MCM-41, Fe₃O₄/MCM-41, and CUR@ Fe₃O₄/MCM-41. The X-ray radiation source is Cu K α band and wavelength ($\lambda=1.541 \text{ \AA}$). The $n\lambda=2d\sin\theta$ and $a_0=2d_{100}/\sqrt{3}$ were used to measure the unit cell & d-spacing. The sample's BET surface area was measured using the Brunauer-Emmett-Teller (BET) method at relative pressures ranging between 0.074-0.293. The mean diameter of the three prepared materials was estimated from the desorption branch of the isotherm test using the Barrett-Joyner-Halenda (BJH) process. The thickness of a pore's wall determines the difference in unit cell property (a_0) & pore diameter (D_p). Infrared spectra FT-IR of MCM-41 in data transmission at ambient conditions ranging around 4000 and 500 cm⁻¹ using Spectrum Two™ (PerkinElmer, USA). The morphology of three samples was studied using scanning electron microscopy (SEM) with a TESCAN MIRA3 (France).

2.5 Curcumin stock solution

A standard CUR stock solution of 100 mg/L was prepared; dissolve 10 mg CUR into 100 ml solvent (ethanol) at 30° C with a stirrer for 20 min. Because CUR has low solubility in water, the co-solvent was used to enable it to dissolve. CUR concentrations (10-100) mg/L were prepared after diluting the stock solution. Using a UV-visible spectrophotometer to plot absorbance against wavelengths, the maximum wavelengths of CUR ($\lambda_{max}=432 \text{ nm}$) appear as peaks.

2.6 Curcumin Loading

The loading of CUR was done using a certain amount of MCM-41 & Fe₃O₄/MCM-41 to 50ml of 30 mg/L CUR concentration and shaken at 270 rpm for 24 h at ambient temperature. Next, CUR loaded on MCM-41, and Fe₃O₄/MCM-41 was centrifuged for 30 minutes at 5000 rpm. Using a syringe filter (0.22 μ), the drug supernatant was extracted into quartz. The concentration of the drug was measured using a UV-visible spectrophotometer by seeing the major peak at 432nm, which

coincides with the absorption limit of CUR. After subtracting the amount of CUR contained in the supernatant from the amount of CUR present before adding the adsorbent material, the amount of loaded CUR was determined using the equation below [19].

$$\text{Drug Loading (DL)(\%)} = \frac{M2-M1}{M3} \times 100 \quad (1)$$

Where: $M2$ is the weight of adsorbent after loading, $M1$ represents the weight of adsorbent before loading & $M3$ is the initial weight of CUR in solution.

2.7 Isotherm model for adsorption

The linearized models of Langmuir, Freundlich, & Temkin were utilized to investigate adsorption loading. The Langmuir linear form is given by Eq. 2. Where q_e (in mg/g) and q_m (in mg/g) denoted the equilibrium & maximum adsorption capacity. The q_m & K_L constant was obtained from the slope and intercept of the linear plot of Eq.2. C_{eq} (in mg/L) is the concentration of the drug at an equilibrium state, K_L (in L/mg) is the adsorption energy constant. Eq. 3 illustrates the Freundlich model. The parameters K_f and $1/n$ represent the adsorption capacity and intensity in this equation. The value of this parameter can be calculated from the slope & intercept of the linear plot of Eq.3. The Temkin linear form shows in Eq. 4. The equilibrium bindings constant K_T indicates the optimal binding energy (L/g), while the b_T represents the Temkin constant. Therefore, the slope and intercept of the linear plot of Eq.4 can be used to get the values of B & K_T .

$$\text{Langmuir isotherm model: } \frac{C_{eq}}{q_e} = \frac{1}{q_m} C_{eq} + \frac{1}{K_L q_m} \quad (2)$$

$$\text{Freundlich Isotherm Model: } \ln q_e = \ln K_f + \frac{1}{n} \ln C_{eq} \quad (3)$$

$$\text{Temkin Isotherm Model: } q_e = \frac{RT}{b_T} \ln K_T + \frac{RT}{b_T} \ln C_{eq} \quad \text{Where } \frac{RT}{b_T} = B \quad (4)$$

$$\text{The dimensionless equilibrium parameter } R_L \text{ is defined as follows: } R_L = \frac{1}{1+K_L C_0} \quad (5)$$

Where K_L represents the Langmuir constant, C_0 is the largest initial drug concentration in (mg/L), R_L value shows if the isotherm is favorable. ($R_L < 1$), unfavorable ($R_L > 1$), irreversible ($R_L = 0$), or linear ($R_L = 1$) [17].

2.8 Kinetic adsorption

The kinetics of CUR adsorption on MCM-41 & $\text{Fe}_3\text{O}_4/\text{MCM-41}$ were investigated with pseudo-first & pseudo-second-order kinetics models, as shown in the following equations.

$$\text{Pseudo-First Order: } \log(q_e - q_t) = \log q_e - \frac{k_1}{2.303} t \quad (6)$$

$$\text{Pseudo-Second Order: } \frac{t}{q_t} = \frac{1}{k_2 q_e^2} + \frac{1}{q_e} t \quad (7)$$

Where q_e & q_t are the adsorption capabilities at equilibrium state & at time t in mg/g, respectively. The pseudo-first-order & pseudo-second-order adsorption rate constants are k_1 (min^{-1}) and k_2 ($\text{g/mg}\cdot\text{min}$), respectively. The values of the parameters k_1 , q_e , and k_2 can be calculated from the slope and intercept of the linear plot of Eq.6 & 7, respectively [20].

2.9 Curcumin Released

The release of CUR from MCM-41 and $\text{Fe}_3\text{O}_4/\text{MCM-41}$ was achieved in a laboratory setting at different time intervals. First, the Phosphate Buffer Solution was prepared. One liter of deionized water was mixed with 0.888 g of KH_2PO_4 (M.W:136.086 g/mole) & 16.282 g of K_2HPO_4 (M.W:174.18 g/mole). Ion concentrations and human blood plasma were simulated; the pH of the solution was changed to 7.4 to mimic the pH of the intestine. To mimic body temperature, 0.12g of CUR@MCM-41 and 0.1g of CUR@ $\text{Fe}_3\text{O}_4/\text{MCM-41}$ were soaked in 100 ml of PBS with pH 7.4 and stirred at 500 rpm and 37°C. A syringe was used to extract the solution into a quartz cuvette. A UV-visible spectrophotometer was used to measure the amount of CUR emitted. The released % of CUR was determined using the equation below [21].

$$\text{Release (\%)} = \frac{\text{The weight of CUR in PBS media}}{\text{The weight of CUR in MSNs}} \times 100\% \quad (8)$$

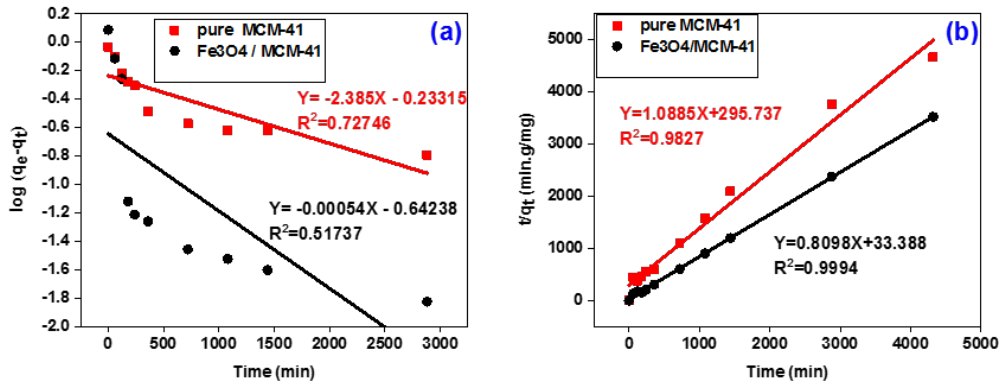


Figure 7: (a) Pseudo-first order (b) Pseudo- second order kinetics model for loading CUR on MCM-41 and Fe₃O₄/MCM-41

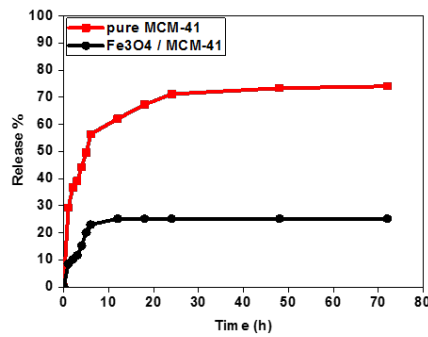


Figure 8: CUR release percentage from MCM-41 and Fe₃O₄/MCM-41 in PBS solution at pH= 7.4.

Table 1: Structure properties of MCM-41, Fe₃O₄/MCM-41, & CUR@Fe₃O₄/MCM-41.

Material	S _{BET} (m ² /g)	V _p (cm ³ /g)	D _{BjH} (nm)	Particle Size (nm)	d ₁₀₀ (nm) XRD	a ₀ (nm) XRD	W _t (nm)	O Wt.% EDX	Si Wt.% EDX
MCM-41	1200	0.7395	3.193	5.5514	3.851	4.447	1.254	48.68	42.43
Fe ₃ O ₄ /MCM-41	1090	0.669	2.855	5.6036	3.851	4.447	1.592	45.64	30.51
CUR@Fe ₃ O ₄ /MCM-41	1028	0.564	2.737	5.8330	3.851	4.447	1.895	43.86	27.35

V_p refers to pore volume, (S_{BET}): BET surface area, a₀ = (2* d₁₀₀ /√3): center-center distance, d₁₀₀: spacing of d (1 0 0), (D_{BjH}): pore diameter W_t: wall thickness, calculated using the formula (a₀ - D_{BjH})

Table 2: Isotherm factors for CUR loading by MCM-41 and Fe₃O₄/MCM-41 with the correlation coefficient.

Material	Langmuir				Freundlich			Temkin		
	Q _{maxi} mg/g	K _L (L/mg)	R _L	R ²	K _f (mg/g)	n	R ²	K _T (L/mg)	B	R ²
MCM-41	16.96	0.0064	0.7575	0.9348	0.133	1.130	0.9992	0.1854	1.637	0.95
Fe ₃ O ₄ /MCM-41	2.635	0.069	0.2239	0.8444	0.610	3.285	0.7751	1.154	0.495	0.70

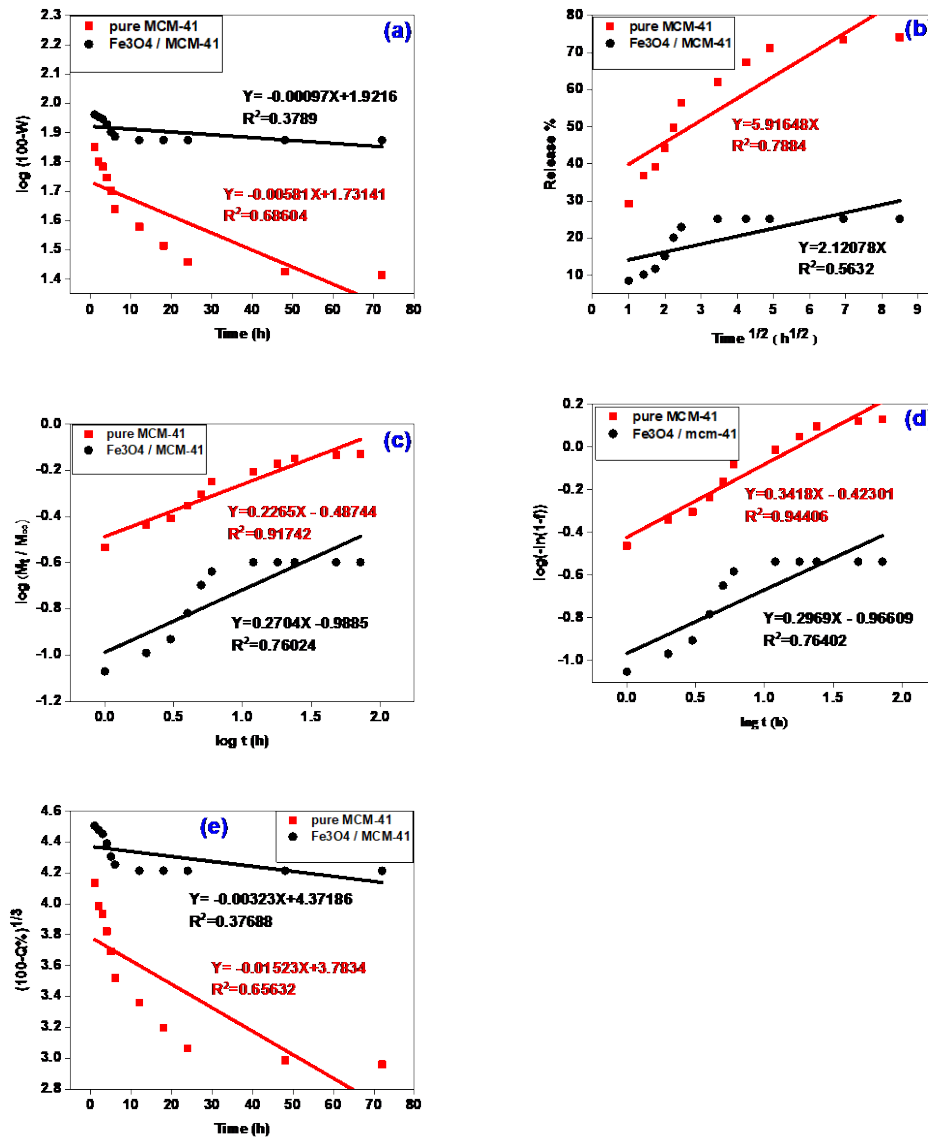


Figure 9: CUR kinetics release model (a) first-order, (b) Higuchi, (c) Korsmeyer-Peppas, (d) Weibull, and (e) Hixson and Crowell.

3. Results and Discussion

3.1 X-Ray Diffraction Pattern

The MCM-41, Fe₃O₄/MCM-41, & CUR@Fe₃O₄/MCM-41 XRD patterns were depicted in Figure 2. In this Figure, pure MCM-41 has a high diffraction peak at 2 θ of 2.3 & two weak peaks at 2 θ of 4.1 and 5, respectively, which can be labeled as (1 0 0), (1 1 0), & (2 0 0) surfaces. This refers to the hexagonally organized MCM-41 silica with highly nanostructured channels. After adding Fe₃O₄ to the MCM-41 matrix and loading with CUR, the (1 0 0) peak can also be seen, indicating that the ordered mesoporous structure is preserved as iron species are introduced. The removal of (1 1 0) & (2 0 0) peaks, on the other hand, suggests that Fe₃O₄/MCM-41 & CUR@Fe₃O₄/MCM-41 have some iron loading content. The unit cell value a_0 is calculated from the diffraction angle using equation $a_0 = (2 \cdot d_{100} \cdot \sqrt{3})$. The determined d_{100} and a_0 values are seen in Table 1 [22]. In Table 1, there is a decrease in the surface area, a decrease in the pore diameter and an increase in the wall thickness due to the loading on the surface of the mesoporous materials and within the pore diameter.

Table 3: Parameters and constant for pseudo-first-order & pseudo-second-order kinetic models for the CUR loading on the MCM-41 and Fe₃O₄/MCM-41.

Adsorbent	Pseudo-first order				Pseudo-second order		
	q _e (exp) mg/g	q _e mg/g	K ₁ min ⁻¹	R ²	q _e mg/g	K ₂ g/mg. min	R ²
MCM-41	0.925	0.5845	5.4926	0.7274	0.9186	0.004	0.9827
Fe ₃ O ₄ /MCM-41	1.225	0.2278	0.0012	0.5173	1.234	0.0196	0.9994

Table 4: CUR release kinetic parameters from MCM-41 and Fe₃O₄/MCM-41 to PBS at pH=7.4.

Drug	First order		Higuchi		Weibull		Korsmeyer-peppase			Hixson - Crowell	
	K _t (h ⁻¹)	R ²	K _H (h ^{1/2})	R ²	m	R ²	K (h ⁻¹)	n	R ²	K _{HC} (h ⁻¹)	R ²
CUR@MCM-41	0.0058	0.686	5.916	0.788	0.341	0.944	0.325	0.226	0.917	0.0152	0.656
CUR@Fe ₃ O ₄ /MCM-41	0.0009	0.379	2.120	0.563	0.297	0.764	0.103	0.270	0.760	0.0032	0.377

3.2 FTIR Spectra

The functional group of the three materials, MCM-41, Fe₃O₄/MCM-41 & CUR@Fe₃O₄/MCM-41, was verified using the FTIR spectra. For pure MCM-41 asymmetrical stretch of silanol group Si-OH can be attributed to a sharp band around 1075 cm⁻¹ and a shoulder around 1243 cm⁻¹, representing the fingerprint region of the MCM-41. The stretching bands of the silanol group were seen at (1046-1090) cm⁻¹ and 1092 cm⁻¹ in Fe₃O₄/MCM-41 & CUR@Fe₃O₄/MCM-41 samples, respectively. The band at 972 cm⁻¹ (silanol groups) decreases in intensity, indicating that the Fe₃O₄ adsorbed onto the silica surface co-occurs with the disappearance of hydroxyl groups. Furthermore, the Fe₃O₄/MCM-41 FTIR spectrum was magnified from 400 to 1000 cm⁻¹, and a weak band at 588 cm⁻¹ coming from Fe-O vibrations was discovered. The absence of a significant Fe-O signal in the FTIR spectra is likely related to the low amount of Fe₃O₄ and the interaction between Fe & Si atoms. In contrast, iron oxide nanoparticles are very firmly attached to the interior wall of silica Nanopores. The absorption bands that corresponded to the characteristics of aliphatic groups were present in Fe₃O₄/MCM-41, about 2922 -2853 cm⁻¹, but disappeared in CUR@Fe₃O₄/MCM-41. As shown in Figure 3, there is a slight difference between these three materials [22].

3.3 Scanning Electron Microscopy (SEM)

SEM photo of manufactured MCM-41, Fe₃O₄/MCM-41, & CUR @ Fe₃O₄/MCM-41, was shown in Figure 4. This figure demonstrates the material's linear nano-structure & uniform structure. Furthermore, the produced material, agglomeration spherical particles with smooth surfaces, were observed in Figure 4 (a) [23]. Figure 4 (b) was shown that Fe₃O₄ loading did not affect the mesopore structure. While the particle size, morphology, and channels in Figure 4 (c) differed from those in other images, indicating the existence of CUR. The existence of O and Si is measured by EDX & displayed in Table 1 [24].

3.4 Curcumin Loading

1. The effect of the carrier dose

The drug loading efficiency DL% of pure MCM-41 and Fe₃O₄/MCM-41 was increased with increasing the dose for CUR loaded, as seen in Figure 5(a). From this figure, the DL% varied from 5.5 to 18.3 % and from 7.7 to 17.76 % when the dosage was increased from 20 to 200 mg for each MCM-41 & Fe₃O₄/MCM-41, respectively. The results revealed that drug DL% reached equilibrium at 120 mg & 100 mg with rising carrier doses at a constant concentration of CUR 10 mg/L for MCM-41 and Fe₃O₄/MCM-41, respectively. It is thought to be the best dosage for the carrier. The drug loading equilibrium because the driving force of the CUR molecules reduced as increased carriers dosage, leading to an increased number of adsorption sites, higher surface area, and pore size. MCM-41 & Fe₃O₄/MCM-41 have a difference in DL% of about 2.7 %, insignificant. As demonstrated in Table 1, the discrepancy could be attributed to Fe particle dispersion in MCM-41 pores, resulting in a reduction in Fe₃O₄/MCM-41 total surface area [25].

2. Effect of initial curcumin concentration

The influence of the initial concentration of CUR on DL% was evaluated, as depicted in Figure 5(b). In this figure, CUR concentrations were altered between (10-50) mg/L to see the influence of initial concentration on DL%, associated with the diffusion process & CUR concentration. When the initial concentration was increased from 10 to 50 mg/L, the DL% reduced from 20 to 17.36 % and from 24.2 to 9.08 % for each MCM-41 and Fe₃O₄/MCM-41, respectively. The decrease in DL% can be explained by the fact that all Fe₃O₄/MCM-41 active sites were restricted & were saturated above a specific concentration. The first quantitative relationship between CUR particles and feasible loading sites was weak at low concentrations. CUR nanoparticles reached many mesoporous regions, resulting in a higher DL% [26].

3. Effect of pH

The relationship between DL% and pH on MCM-41 & Fe₃O₄/MCM-41 was represented in Figure 5(c). The pH was altered from 2 - 10, and CURs DL% was increased from 14.23 % to 21.3 % and from 17.28 % to 24.67 %, for MCM-41 and

Fe₃O₄/MCM-41, respectively. This rise in DL% is due to the electrostatic attraction force between the CUR compounds with MCM-41 and Fe₃O₄/MCM-41. As a result the DL% was found to be 20 & 24.2 % at pH= 7.5, and 17.28 & 24.67 % at pH= 10 for MCM-41 and Fe₃O₄/MCM-41, respectively. Therefore the best optimum pH was chosen at pH=7.5 because the difference among DL% values is tiny and pH at 7.5 indicates the steady-state [27].

4. Effect of contact time

The effect of contact time on CUR loading is depicted in Figure 5(d). In this figure, CUR loading performance was high within the first 12 h for MCM-41 and three h for Fe₃O₄/MCM-41, then maintained constant for the following hours. At the beginning of the process, there was an abundance of existing mesoporous sites on the CUR load surface. Due to overload, the last accessible mesoporous sites were challenging to occupy as the contact time increased longer, implying that MCM-41 and Fe₃O₄/MCM-41 were attracted by CUR nanoparticles. This could be due to a limitation of loaded sites available at the end of the procedure, causing loading performance to stay constant [28].

3.5 Adsorption isotherms

The linearized forms of the Langmuir, Freundlich, & Temkin equations were presented in Figure 6 (a-c) to study the adsorbed process. Table 2 shows the isotherm results for these three models and values of the correlation coefficient (R²). The R² value of 0.9992 for pure MCM-41, the Freundlich isotherm offered the most excellent experimental results, whereas Fe₃O₄/MCM-41 fit the Langmuir isotherm with an R² value of 0.8444. The non-dimensional separation factor R_L was calculated from Eq. 5. It was found to be 0.757 and 0.223 for MCM-41 and Fe₃O₄/MCM-41, respectively. As indicated by the R_L, the Langmuir isotherm was favorable because the value of R_L was less than 1 [29].

3.6 Kinetic of adsorption

The kinetics of CUR loading on pure MCM-41 and Fe₃O₄/MCM-41 were investigated using pseudo-first and pseudo-second-order kinetics models, as illustrated in Figure 7 (a & b). Table 3 presents the correlation coefficients and values of the pseudo-first-order and pseudo-second-order equation parameters and the effects of the linearized results for both models for CUR adsorption by two carriers. The experimental data was the best fit by the pseudo-second-order kinetic model because the determination coefficient (R²) was closer to one equal 0.9827 and 0.9994 for MCM-41 and Fe₃O₄/MCM-41, respectively. Furthermore, the measured and experimental values of q_e were highly similar [17].

3.7 Releasing of curcumin

The dissolving analysis is a valuable tool for improving & monitoring a medication's efficacy. Figure 8 shows the percentage of CUR released from MCM-41 and Fe₃O₄/MCM-41 samples in a phosphate buffer solution at a pH of 7.4 and temperature of 37°C, similar to the human body. At the start of the dissolution, a primary driving force in between concentrations at the MCM-41 and Fe₃O₄/MCM-41 surfaces and in the media was high, resulting in a small percentage of CUR released. Then, as the time of dissolution increased, the CUR release steadily increased until equilibrium was reached. Because at pH 7.4, the decrease in H⁺ concentration caused the hydrogen bonds among MCM-41 and Fe₃O₄/MCM-41 with the CUR molecule to decrease. After 72 h, the CUR release could be as high as 74.1 & 25.19% for MCM-41 and Fe₃O₄/MCM-41, respectively [30].

3.8 Kinetic model for release of curcumin

The process of CUR release was investigated using a variety of kinetic models, including the first order, Weibull, Hixson-Crowell, Korsmeyer-Peppas, and Higuchi models, as shown in the following equations:

$$\text{First-order: } \log(100 - W) = \log 100 - K_1 t \quad (9)$$

$$\text{Higuchi Kinetics: } W = KHt^{\frac{1}{2}} \quad (10)$$

$$\text{Korsmeyer-peppas model: } \frac{Mt}{M_{\infty}} = Kt^n \quad (11)$$

$$\text{Weibull model: } \log[-\ln(1 - f)] = m \log t - \ln t_0 \quad (12)$$

$$\text{Hixson - Crowell model: } (100 - Q)^{1/3} = 100/3 - K_{HC} t \quad (13)$$

Where W denotes the cumulative release percentage. f is the cumulative quantity fraction of CUR released. The CUR rate constants in the first order, Higuchi and Weibull models are K_1 , KH , and m , respectively. The CUR fraction (Mt/M_{∞}) was determined in the dissolving media. K refers to the drug's structural and geometric features. Q is the drug's percent at time t . Hixson-Crowell dissolving rate constant (K_{HC}). It is necessary to calculate the drug's transport mechanism. The Korsmeyer-Peppas kinetic model was used to calculate the diffusion exponent n . The Fickian diffusion is characterized when the value of $n \leq 0.5$, and the anomalous mechanism is characterized when n is between 0.5 and 1. There are two types of diffusion described by Fick's laws: Fickian and Non-Fickian Diffusion. Non-Fickian diffusion does not follow Fickian laws, but Fickian diffusion does. The presence or absence of boundaries distinguishes Fickian and Non-Fickian Diffusion. Non-Fickian diffusion has a clear boundary separating the loaded drug area, whereas Fickian diffusion has none. Figure 9 (a-e) shows how the

experimental data were fitted using the equations (9–13) above to estimate the CUR's releasing process. Table 4 presents the parameter estimates for all released CUR kinetic models. The supplied data was fitted with a strong linear fit using the Weibull model. The correlation coefficient R^2 equals 0.944 and 0.764 for MCM-41 and $\text{Fe}_3\text{O}_4/\text{MCM-41}$, respectively. The estimated values of n based on the mentioned values indicate the Fickian diffusion because it is less than 0.5. Free drug molecules were leached from the MCM-41 and $\text{Fe}_3\text{O}_4/\text{MCM-41}$'s pore, resulting in drug diffusion out of the system's microchannels, causing the immediate release. As a result, the CUR slowly dissolved into the liquid phase [31].

4. Conclusions

Curcumin's solubility can be improved by using nanotechnology or modifying its functional groups. The present study used the (IWI) process to successfully manufacture ordered mesoporous silica particles surface modification with Fe_3O_4 nanoparticles ($\text{Fe}_3\text{O}_4/\text{MCM-41}$). The addition of Fe_3O_4 nanoparticles did not affect the silica particles' order pores or their large surface area. The prepared material MCM-41 and $\text{Fe}_3\text{O}_4/\text{MCM-41}$ was loaded with CUR. The optimum efficiency of CUR loading was achieved at 15.78 and 22.98% for pure MCM-41 and $\text{Fe}_3\text{O}_4/\text{MCM-41}$, respectively. The adsorption process fitted to the Freundlich isotherm with a higher correlation coefficient (R^2) 0.9992 for pure MCM-41 and Langmuir isotherm for $\text{Fe}_3\text{O}_4/\text{MCM-41}$ with R^2 equal to 0.8444. CUR adsorption kinetics best describes the pseudo-second-order model with $R^2=$ 0.9827 and 0.9994 for MCM-41 and $\text{Fe}_3\text{O}_4/\text{MCM-41}$, respectively. The higher CUR release in PBS media with a pH of 7.4 for 72 h was observed 74.1% and 25.19 % for MCM-41 & $\text{Fe}_3\text{O}_4/\text{MCM-41}$, respectively. The kinetics of CUR released from MCM-41 & $\text{Fe}_3\text{O}_4/\text{MCM-41}$ were described using the Weibull model with R^2 0.944 and 0.764 for MCM-41 & $\text{Fe}_3\text{O}_4/\text{MCM-41}$, respectively.

Acknowledgment

The authors would like to express their gratitude to the Department of Chemical Engineering, University of Technology-Iraq, Baghdad, Iraq.

Author contribution

All authors contributed equally to this work.

Funding

This research received no specific grant from any funding agency in the public, commercial, or not-for-profit sectors.

Data availability statement

The data that support the findings of this study are available on request from the corresponding author.

Conflicts of interest

The authors declare that there is no conflict of interest.

References

- [1] R. R. Castillo, M. Colilla, and M. Vallet-Regí, Advances in mesoporous silica-based nanocarriers for co-delivery and combination therapy against cancer, *Expert Opin. Drug Deliv.*, 14 (2017) 229–243. <https://doi.org/10.1080/17425247.2016.1211637>
- [2] T. M. Albayati and A. A. A. Jassam, Synthesis and characterization of mesoporous materials as a carrier and release of prednisolone in drug delivery system, *J. Drug Deliv. Sci. Technol.*, 53 (2019) 101176. <https://doi.org/10.1016/j.jddst.2019.101176>
- [3] L. Slika, A. Moubarak, J. Borjac, E. Baydoun, D. Patra, Preparation of curcumin-poly (allyl amine) hydrochloride based nanocapsules: Piperine in nanocapsules accelerates encapsulation and release of curcumin and effectiveness against colon cancer cells, *Mater. Sci. Eng. C*, 109 (2020) 110550. <https://doi.org/10.1016/j.msec.2019.110550>
- [4] D. Zhang, M. Fu, S.-H. Gao, J.-L. Liu, Curcumin and diabetes: a systematic review.: Evidence-based Complement. Altern. Med., 2013 (2013)16. <https://doi.org/10.1155/2013/636053>
- [5] M. Popova, I. Trendafilova, Á. Szegedi, J. Mihály, P. Németh, S.G. Marinova, H.A. Aleksandrov and G.N. Vayssilov, Experimental and theoretical study of quercetin complexes formed on pure silica and Zn-modified mesoporous MCM-41 and SBA-16 materials, *Microporous Mesoporous Mater.*, 228 (2016) 256–265. <https://doi.org/10.1016/j.micromeso.2016.04.001>
- [6] D. B. Abed, Removal of Cobalt (Co(II)) from Aqueous Solution by Amino Functionalized SBA-15, *Eng. Technol. J.*, 36 (2018) 703–708. <https://doi.org/10.30684/etj.36.7a.1>
- [7] M. Sari Yilmaz, A. Palantoken, and S. Piskin, Release of flurbiprofen using of SBA-15 mesoporous silica: Influence of silica sources and functionalization, *J. Non. Cryst. Solids*, 437 (2016) 80–86. <https://doi.org/10.1016/j.jnoncrysol.2016.01.020>

- [8] H. F. Alazzawi, I. K. Salih, and T. M. Albayati, Drug delivery of amoxicillin molecule as a suggested treatment for covid-19 implementing functionalized mesoporous SBA-15 with aminopropyl groups, *Drug Deliv.*, 28 (2021) 856–864. <https://doi.org/10.1080/10717544.2021.1914778>
- [9] M. Vallet-Regi, A. Rámila, R. P. Del Real, and J. Pérez-Pariente, A new property of MCM-41: Drug delivery system, *Chem. Mater.*, 13 (2001) 308–311. <https://doi.org/10.1021/cm0011559>
- [10] A. S. Tsybko, T. G. Amstislavskaya, G. V. Kontsevaya, L. A. Gerlinskaya, Effect of chronic inhalation of silicon dioxide nanoparticles (Tarkosil 25) on the expression of key genes of the serotonergic system in the mouse brain, *Nanotechnologies Russ.*, 9 (2014) 213–218. <https://doi.org/10.1134/S1995078014020177>
- [11] C. L. Lay, H. Q. Liu, D. Wu, and Y. Liu, Poly(ethylene glycol)-graft-hollow silica vesicles for drug delivery, *Chem. - A Eur. J.*, 16 (2010) 3001–3004. <https://doi.org/10.1002/chem.200903291>
- [12] S. K. Natarajan and S. Selvaraj, Mesoporous silica nanoparticles: Importance of surface modifications and its role in drug delivery, *RSC Adv.*, 4 (2014) 14328–14334. <https://doi.org/10.1039/c4ra00781f>
- [13] M. Shinkai, Functional magnetic particles for medical application, *J. Biosci. Bioeng.*, 94 (2002) 606–613. [https://doi.org/10.1016/S1389-1723\(02\)80202-X](https://doi.org/10.1016/S1389-1723(02)80202-X)
- [14] N. V. Mdlovu, K. S. Lin, M. T. Weng, C. C. Hsieh, Y. S. Lin, and M. J. Carrera Espinoza, In vitro intracellular studies of pH and thermo-triggered doxorubicin conjugated magnetic SBA-15 mesoporous nanocarriers for anticancer activity against hepatocellular carcinoma, *J. Ind. Eng. Chem.*, 102 (2021) 1–16. <https://doi.org/10.1016/j.jiec.2021.06.004>
- [15] L. Harini, B. Karthikeyan, S. Srivastava, S.B. Suresh, C. Ross, G. Gnanakumar, S. Rajagopal, K. Sundar and T. Kathiresan, Polyethylenimine-modified curcumin-loaded mesoporous silica nanoparticle (MCM-41) induces cell death in MCF-7 cell line, *IET Nanobiotechnology*, 11 (2017) 57–61. <https://doi.org/10.1049/iet-nbt.2016.0075>
- [16] N. Taebnia, D. Morshedi, S. Yaghmaei, F. Aliakbari, F. Rahimi, and A. Arpanaei, Curcumin-Loaded Amine-Functionalized Mesoporous Silica Nanoparticles Inhibit α -Synuclein Fibrillation and Reduce Its Cytotoxicity-Associated Effects, *Langmuir*, 32 (2016) 13394–13402. <https://doi.org/10.1021/acs.langmuir.6b02935>
- [17] T. M. Albayati, G. M. Alwan, and O. S. Mahdy, High performance methyl orange capture on magnetic nanoporous MCM-41 prepared by incipient wetness impregnation method, *Korean J. Chem. Eng.*, 34 (2017) 259–265. <https://doi.org/10.1007/s11814-016-0231-2>
- [18] S. Liu, K. Yao, L.-H. Fu, and M.-G. Ma, Selective synthesis of Fe₃O₄, γ -Fe₂O₃, and α -Fe₂O₃ using cellulose-based composites as precursors, *RSC Adv.*, 6 (2016) 2135–2140. <https://doi.org/10.1039/C5RA22985E>
- [19] E. Ahmadi, N. Dehghannejad, S. Hashemikia, M. Ghasemnejad, and H. Tabebordbar, Synthesis and surface modification of mesoporous silica nanoparticles and its application as carriers for sustained drug delivery, *Drug Deliv.*, 21 (2014) 164–172. <https://doi.org/10.3109/10717544.2013.838715>
- [20] T. M. Albayati and K. R. Kalash, Polycyclic aromatic hydrocarbons adsorption from wastewater using different types of prepared mesoporous materials MCM-41 in batch and fixed bed column, *Process Saf. Environ. Prot.*, 133 (2020) 124–136. <https://doi.org/10.1016/j.psep.2019.11.007>
- [21] M. M. Ayad, N. A. Salahuddin, A. A. El-Nasr, and N. L. Torad, Amine-functionalized mesoporous silica KIT-6 as a controlled release drug delivery carrier, *Microporous Mesoporous Mater.*, 229 (2016) 166–177. <https://doi.org/10.1016/j.micromeso.04.029>
- [22] L. Le Yu and H. Bi, Facile synthesis and magnetic property of iron oxide/MCM-41 mesoporous silica nanospheres for targeted drug delivery, *J. Appl. Phys.*, 111 (2012) 5–8. <https://doi.org/10.1063/1.3676203>
- [23] J.A. Costa, A.C. Garcia, D.O. Santos, V.H. Sarmiento, A.L. Porto, M.E.D. Mesquita and L.P. Romão, A new functionalized MCM-41 mesoporous material for use in environmental applications, *J. Braz. Chem. Soc.*, 25 (2014) 197–207. <https://doi.org/10.5935/0103-5053.20130284>
- [24] Y. Guo, B. Chen, Y. Zhao, and T. Yang, Fabrication of the magnetic mesoporous silica Fe-MCM-41-A as efficient adsorbent: performance, kinetics and mechanism, *Sci. Rep.*, 11 (2021) 1–12. <https://doi.org/10.1038/s41598-021-81928-8>
- [25] A. M. Alkafajy and T. M. Albayati, High performance of magnetic mesoporous modification for loading and release of meloxicam in drug delivery implementation, *Mater. Today Commun.*, 23 (2019) 100890. <https://doi.org/10.1016/j.mtcomm.100890>
- [26] Y. Shi and R. Crawfis, Group tactics utilizing suppression and shelter, *Proc. CGAMES 2014 USA - 19th Int. Conf. Comput. Games AI, Animat. Mobile, Interact. Multimedia, Educ. Serious Games, Im* (2014) 20–27. <https://doi.org/10.1109/CGames.6934139>
- [27] A. Salis, D.F. Parsons, M. Bostrom, L. Medda, B. Barse, B.W. Ninham and M. Monduzzi, Ion specific surface charge density of SBA-15 mesoporous silica, *Langmuir*, 26 (2010) 2484–2490. <https://doi.org/10.1021/la902721a>

- [28] D. Zhao, J. Feng, Q. Huo, N. Melosh, G.H. Fredrickson, B.F. Chmelka and G.D. Stucky, Triblock Copolymer Syntheses of Mesoporous Silica with Periodic 50 to 300 Angstrom Pores, *Science*, 279 (2016) 548–552. <https://doi.org/10.1126/science.279.5350.548>
- [29] Y. Yao, H. Bing, X. Feifei, and C. Xiaofeng, Equilibrium and kinetic studies of methyl orange adsorption on multiwalled carbon nanotubes, *Chem. Eng. J.*, 170 (2011) 82–89. <https://doi.org/10.1016/j.cej.2011.03.031>
- [30] T. M. Albayati, I. K. Salih, and H. F. Alazzawi, Synthesis and characterization of a modified surface of SBA-15 mesoporous silica for a chloramphenicol drug delivery system, *Heliyon*, 5 (2019) e02539. <https://doi.org/10.1016/j.heliyon.2019.e02539>
- [31] T. M. Albayati, A. A. A. Jassam, Experimental Study of Drug Delivery system for Prednisolone Loaded and Experimental Study of Drug Delivery system for Prednisolone Loaded and Released by Mesoporous Silica MCM-41, *Al-Khwarizmi Eng. J.*, 15 (2019) 117–124. <https://doi.org/10.22153/kej.2019.06.004>